Molecular and Cellular Probes 28 (2014) 175–180

Contents lists available at ScienceDirect

Molecular and Cellular Probes

journal homepage: www.elsevier.com/locate/ymcpr

An image analysis method to quantify CFTR subcellular localization

Lucilla Pizzo [a], María Inés Fariello [a,b], Paola Lepanto [a], Pablo S. Aguilar [a], Arlinet Kierbel [a,c,*]

[a] Institut Pasteur de Montevideo, Montevideo 11400, Uruguay
[b] IMERL, Facultad de Ingeniería, Universidad de la República, Montevideo, Uruguay
[c] Instituto de Investigaciones Biotecnológicas Dr. Rodolfo A. Ugalde (IIB-INTECH), Universidad Nacional de San Martín, Consejo Nacional de Investigaciones Científicas y Técnicas (UNSAM-CONICET), San Martín, Buenos Aires, Argentina

ARTICLE INFO

Article history:
Received 22 November 2013
Received in revised form
11 February 2014
Accepted 12 February 2014
Available online 21 February 2014

Keywords:
CFTR
Apical
Image analysis
Deconvolution

ABSTRACT

Aberrant protein subcellular localization caused by mutation is a prominent feature of many human diseases. In Cystic Fibrosis (CF), a recessive lethal disorder that results from dysfunction of the Cystic Fibrosis Transmembrane Conductance Regulator (CFTR), the most common mutation is a deletion of phenylalanine-508 (pF508del). Such mutation produces a misfolded protein that fails to reach the cell surface. To date, over 1900 mutations have been identified in CFTR gene, but only a minority has been analyzed at the protein level. To establish if a particular CFTR variant alters its subcellular distribution, it is necessary to quantitatively determine protein localization in the appropriate cellular context. To date, most quantitative studies on CFTR localization have been based on immunoprecipitation and western blot. In this work, we developed and validated a confocal microscopy-image analysis method to quantitatively examine CFTR at the apical membrane of epithelial cells. Polarized MDCK cells transiently transfected with EGFP-CFTR constructs and stained for an apical marker were used. EGFP-CFTR fluorescence intensity in a region defined by the apical marker was normalized to EGFP-CFTR whole cell fluorescence intensity, rendering "apical CFTR ratio". We obtained an apical CFTR ratio of 0.67 ± 0.05 for wtCFTR and 0.11 ± 0.02 for pF508del. In addition, this image analysis method was able to discriminate intermediate phenotypes: partial rescue of the pF508del by incubation at 27 °C rendered an apical CFTR ratio value of 0.23 ± 0.01. We concluded the method has a good sensitivity and accurately detects milder phenotypes. Improving axial resolution through deconvolution further increased the sensitivity of the system as rendered an apical CFTR ratio of 0.76 ± 0.03 for wild type and 0.05 ± 0.02 for pF508del. The presented procedure is faster and simpler when compared with other available methods and it is therefore suitable as a screening method to identify mutations that completely or mildly affect CFTR processing. Moreover, it could be extended to other studies on the biology underlying protein subcellular localization in health and disease.

1. Introduction

Subcellular localization is essential for protein function as it determines the access of proteins to interacting partners, integrating these into functional biological networks. Indeed, aberrant protein localization caused by mutation, or by deregulation of components of the trafficking machinery, is a prominent feature of many human diseases as diverse as Alzheimer's disease, kidney stones and cancer [1].

An example of these conditions is Cystic Fibrosis (CF), the most common autosomal recessive lethal disorder among Caucasian populations. This genetic disease results from mutations and consequential dysfunction of the Cystic Fibrosis Transmembrane Conductance Regulator (CFTR) [2,3]. CFTR is a cyclic AMP-dependent chloride channel that localizes at the apical membrane of epithelial cells where it plays a key role in salt and water homeostasis. About 90% of CF cases involve a deletion of phenylalanine-508 (pF508del) [4]. Such mutation produces a misfolded protein that is retained in the endoplasmic reticulum (ER) and degraded, so that a small fraction of translated CFTR reaches the apical surface [5]. At least eighteen other disease-causing mutations have been reported to affect CFTR membrane targeting as well [6–9].

To date, over 1900 mutations have been identified in CFTR gene, but only a minority have been analyzed at the protein level [10,11].

* Corresponding author. Instituto de Investigaciones Biotecnológicas Dr. Rodolfo A. Ugalde (IIB-INTECH), Universidad Nacional de San Martín, Consejo Nacional de Investigaciones Científicas y Técnicas (UNSAM-CONICET), San Martín, Buenos Aires, Argentina.
E-mail address: akierbel@iibintech.com.ar (A. Kierbel).

http://dx.doi.org/10.1016/j.mcp.2014.02.004
0890-8508/

To establish if a particular CFTR variant alters its subcellular distribution, it is necessary to quantitatively determine protein localization in the appropriate cellular context.

Overall, subcellular fractionation and microscopy-based methods have been developed to address the localization of integral membrane proteins. Microscopy-based methods are quite diverse and in most cases they are specific for the cell type and/or membrane compartment that is being addressed. Some methods are based on manual assignment of the membrane compartment [12,13] while others rely on signal filtering and automated segmentation of the compartment of interest [14,15].

Regarding CFTR, most quantitative studies on its localization have been based on immunoprecipitation and western blot. For example, Streptavidin-agarose isolation of biotinylated surface proteins followed by immunoblot analysis with anti-CFTR antibodies has been extensively used [16]. This experimental approach is laborious, time consuming and has low sensitivity. Another method currently employed is the generation of stable cell lines expressing extra-cytoplasmic loop epitope-tagged CFTR variants. These cells lines are then used in ELISA assays which detect surface CFTR by an anti-tag antibody and amplification of the signal by chemo-luminescence or fluorescence reactions [17,18]. Although more sensitive, this method still involves the generation of cell lines and results more appropriate to evaluate potential correctors of the localization defect imposed by pF508del or other known mutations. Recently, Almaca and coworkers have published a fluorescent microscopy quantitative method that uses a CFTR chimera construct carrying mCherry plus a Flag epitope tag in CFTR 4th extracellular loop. In non-permeabilized cells, the Flag tag allows to quantify CFTR localized at the cell surface, while mCherry fluorescence indicates CFTR whole cell expression [19]. While this method provides a good dynamic range, it is limited to proteins with extracellular domains.

Here we report a novel method for assessing apical membrane protein targeting by fluorescence confocal microscopy and quantitative image analysis. We also show that applying deconvolution procedures further increases both the sensitivity and dynamic range of the method. This method is advantageous to determine the effect that clinically-relevant and uncharacterized mutations exert on CFTR localization. In addition, this method can be applied to measure targeting efficiency of any other apical membrane-localized protein of interest.

2. Materials and methods

2.1. Plasmid constructions

Human CFTR cDNA inserted in pGEMHE was kindly provided by Dr. Pablo Artigas (Texas Tech University, Health Sciences Center). Sequence was verified. CFTR cDNA was amplified by polymerase chain reaction (PCR) and cloned into the pEGFP-C1 expression plasmid kindly provided by Ruben Agrelo (Institut Pasteur de Montevideo) to generate the pEGFP-wtCFTR fusion construct as previously reported [20]. A CFTR mutant version lacking the phenylalanine 508 (pEGFP-pF508delCFTR) was constructed using pEGFP-wtCFTR as a template and the site-directed mutagenesis system QuikChange II Kit (Stratagene, Agilent Technologies). Identities of constructed vectors were confirmed by DNA sequencing.

2.2. Cell culture and transfection

Madin-Darby canine kidney (MDCK) cells type II were grown in minimal essential medium (MEM) containing 5% fetal bovine serum (Sigma Aldrich) at 37 °C in a 5% CO_2 atmosphere. Cells were seeded (4.5×10^5 cells per well) on trans-wells (polycarbonate filters, 0.4 μm pore size, Corning Fisher, NY, USA) and were transfected 48 h later using Lipofectamine 2000 and Opti-MEM (Invitrogen, USA) with 1 μg of plasmid constructs. Samples were fixed and processed 24 h after transfection.

2.3. Antibodies and immunofluorescence staining

The apical marker anti gp135 was a gift from G. Ojakian (State University of New York Downstate Medical Center, Brooklyn, NY), the basolateral marker p58 was a gift from K. Matlin (University of Cincinnati, Cincinnati, OH), anti-Calnexin was purchased from AbCam (ab10286). Prior to immunostaining, samples were washed three times with phosphate-buffered saline (PBS) and fixed with 4% paraformaldehyde for 30 min at room temperature. Permeabilization was carried out with 0.1% TritonX100 in PBS for 15 min at 37 °C. Samples were blocked with fish skin gelatin (Sigma) 0.7% in PBS and then incubated over-night at 4 °C with primary antibody (both were diluted 1/3000 in blocking solution). Samples were then incubated for 1 h at 37 °C with secondary antibody (Alexa-543, Invitrogen) and finally 15 min a room temperature with TO-PRO 3 (Invitrogen). Samples were mounted with ProLong® Gold antifade reagent (Invitrogen) and cured for 24 h.

2.4. Confocal laser microscopy and deconvolution

Samples were examined with a confocal microscope (Leica TCS-SP5) using a HCX PL APO 63x/NA1.40 CS oil objective. Images were recorded as 8-bit, and sampled at values smaller than the Nyquist rate (43 nm lateral and 130 nm axial) to prevent aliasing. This was accomplished with an additional 8× zoom and an image resolution of 1024 × 1024 pixels. Confocal stacks were acquired from approximately 20 transfected cells/condition/experiment selected by manual boustrophedon scanning of the entire sample. Blind deconvolution was performed by Huygens Essential software (version 4.2, Scientific Volume Imaging, Hilversum, The Netherlands) using an adaptive point spread function (psf) and the classical maximum likelihood estimation (CMLE) algorithm. The signal to noise ratio employed was 20 and the quality threshold 0.001. A maximum number of 500 iterations were employed. 32bit float deconvolved images were exported as 16-bit TIFF files using the linked scale option to reduce the intensity dynamic range. Image analysis was performed using Image J software.

2.5. Statistics

A simple linear model was applied to the data considering both CFTR genotype and CFTR channel intensity and after verifying that there were not significant differences between same groups from different experiments. Outliers were detected using the Cooks's distance, which identifies leverage points.

Sets of data were compared using the non-parametric Kruskal Wallis test. Significant differences presented a $p < 0.0001$. Statistical analysis were performed using R Software [21]. Results were expressed as mean ± SD of at least three independent experiments.

3. Results and discussion

3.1. Image acquisition

CFTR cellular localization was analyzed in polarized MDCK cells transiently transfected with different EGFP-CFTR constructs and stained with TO-PRO 3 and an antibody against gp-135 to mark nuclear and apical membrane compartments respectively. Isolated cells were xyz imaged from the top to the bottom. Z-stacks

boundaries were consistently defined establishing the basolateral limit one micron below the nuclei and the apical limit two microns above gp135 apical marker. TOPRO-channel was turned off before scanning.

In order to avoid EGFP signal clipping (a large amount of saturated pixels, e.g. pixels with a 255 value in an 8-bit image) acquisition settings (laser power, gain and offset) were first adjusted for the cell that exhibited higher EGFP signal. These acquisition settings were kept invariable for all the cells in that particular experiment making their fluorescence intensities comparable.

3.2. Expression of EGFP-wtCFTR and EGFP-pF508delCFTR in polarized MDCK cells

As shown in Fig. 1, both, p58 and gp135 markers, properly distribute within the basolateral and apical membranes, respectively (Fig. 1A and B). As expected, EGFP-wtCFTR is largely distributed at the apical membrane (Fig. 1A and B) while EGFP-pF508delCFTR shows intracellular localization (Fig. 1C). ER retention of EGFP-pF508delCFTR is clearly visualized on flat MDCK cells grown on coverslips, and immunostained against the ER marker calnexin (Fig. 1D). These results show that EGFP-wtCFTR and EGFP-pF508delCFTR are distributed accordingly with previously reported data, indicating our system is suitable for screening the CFTR localization phenotypes of different mutant alleles.

3.3. Quantification of CFTR subcellular distribution through ImageJ analysis

To quantify the proportion of CFTR residing at the apical membrane, we considered the EGFP-CFTR fluorescence intensity in a region defined by the apical marker gp135. This value was normalized to EGFP-CFTR whole cell fluorescence intensity, rendering "apical CFTR ratio". Such procedure was carried out as follows:

1) Orthogonal planes, perpendicular to the imaged XY planes (Z-axis), were generated for both Alexa-543 (anti-gp135 secondary antibody-conjugated -fluorophore) and EGFP (CFTR) channels, using the ImageJ "Reslice" function (Fig. 2A, left panels).
2) To delineate a region of interest, image thresholding was applied to both channels. Otsu method, a binarization algorithm that

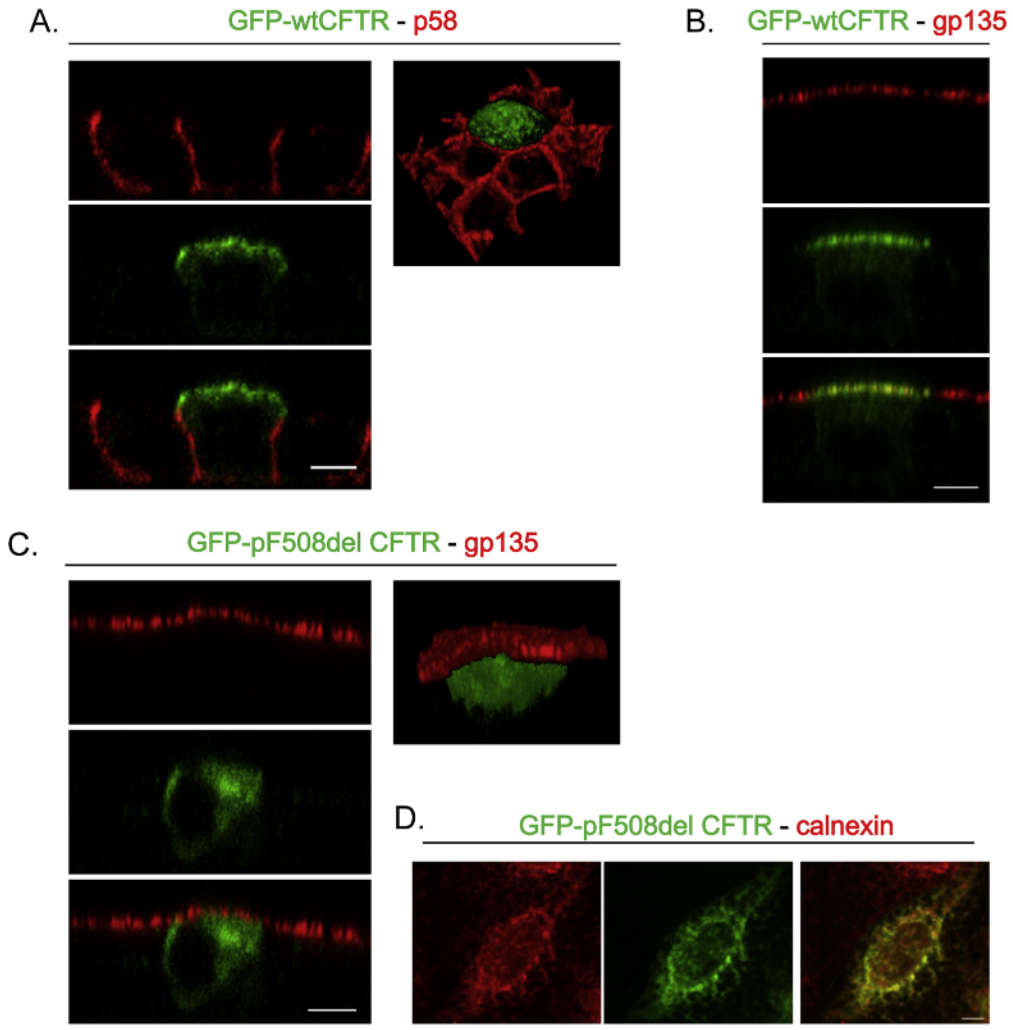

Fig. 1. Expression of GFP-wtCFTR and GFP-pF508delCFTR in polarized MDCK cells. Confocal fluorescence micrographs (xz planes) of polarized MDCK cells transiently expressing GFP-CFTR and stained with the basolateral marker p58 (A) or the apical marker gp135 (B, C). (D) Confocal XY plane of MDCK grown on glass coverslips, transfected with GFP-pF508delCFTR and stained for the endoplasmic reticulum marker calnexin. A, B. GFP-wtCFTR is localized primarily at the apical membrane. C and D. GFP-pF508delCFTR exhibits intracellular localization and resembles the reticular pattern of the endoplasmic reticulum. Three-dimensional reconstructions of field sections containing transfected cells (A, C, right) confirm CFTR localization. Scale bars represent 5 μm.

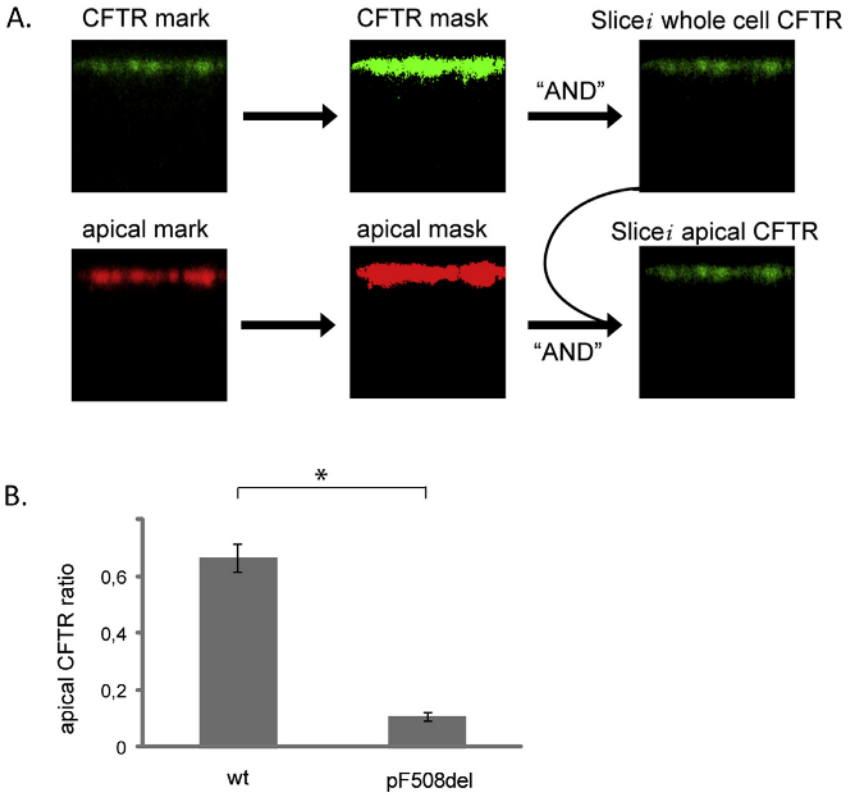

Fig. 2. Quantification of apical CFTR through Image analysis. A. Scheme of the quantitative image analysis procedure (representation showing one slice). B. "Apical CFTR ratio" values for GFP-wtCFTR and GFP-pF508delCFTR. Data represent mean ± standard deviation from at least three independent experiments. *$p < 0.0001$.

finds the threshold value where the sum of foreground and background spreads is at its minimum, was independently applied to each slice of the image [22]. The resulting apical marker channel voxels defined the apical mask whereas the resulting CFTR-channel voxels defined the CFTR mask (Fig. 2A, middle panels).

3) The CFTR mask was intersected with the CFTR signal by the operation "AND" rendering as a result intensities for "whole cell CFTR" for each slice. (Fig. 2A, upper panels)
4) The apical mask was then intersected with "whole cell CFTR" by the operation "AND" rendering as a result intensities for "apical CFTR" for each slice (Fig 2A, curved arrow).
5) The integrated density of the "SUM" projected stacks was calculated for "apical CFTR" and "whole cell CFTR". The proportion of these values determined the "apical CFTR ratio". Thus, apical CFTR ratio = apical CFTR/whole cell CFTR.

The "apical CFTR ratio" was calculated for 95 total cells (EGFP-wtCFTR plus EGPF-pF508delCFTR) within three independent experiments. Five, out of these 95 values were detected as outliers and discarded (all EGFP-wtCFTR). It is worth noting that most of those were also high intensity outliers, suggesting that high expression levels lead to aberrant subcellular localization. If those cases were included "apical CFTR ratio" would be influenced by expression level. We confirmed that the remaining data was within an intensity range where the "apical CFTR ratio" was independent of intensity (Correlation between the ratio and the intensity ~ 0.03).

An average value of (0.67 ± 0.05) was obtained for EGFP-wtCFTR, meaning that 67% of total GFP-CFTR is localized at the apical membrane. For EGFP-pF508delCFTR an average value of (0.11 ± 0.02) was obtained (Fig. 2B). We concluded our method quantitatively renders the difference between apical wtCFTR and pF508delCFTR.

To quantitatively evaluate CFTR mutants delivered to the basolateral membrane [16], an equivalent image analysis procedure can be applied. In such cases, the mask must be generated considering the region defined by a basolateral marker.

3.4. *Deconvolution of confocal images increases the dynamic range of the system*

Subcellular fractionation and purification of the plasma membrane followed by immunodetection studies indicate that 80% of total wild type CFTR is enriched at the plasma membrane fraction whereas the pF508delCFTR variant it is virtually excluded from it [23]. Thus, although our quantification method is able to measure the distribution difference between wild type and mutant versions of CFTR, it still does not entirely reflect the high contrast reported by the mentioned study. More likely, limited axial resolution renders an apical mask that includes a significant part of the cellular interior. As image resolution is critical to this methodology, we decided to further improve it by applying deconvolution. Resolution of both, confocal and widefield images has been shown to significantly increase by deconvolution, an image restoration technique that has also had a profound impact on colocalization studies [24]. For membrane localization studies, the application of this image restoring calculation would be especially pertinent, due to the restricted region under study.

We applied blind deconvolution to both Alexa543 and GFP channels considering the following parameters:

a) PSF: The mismatch between the immersion (refractive index $n = 1.42$) and mounting media ($n = 1.518$) gives spherical

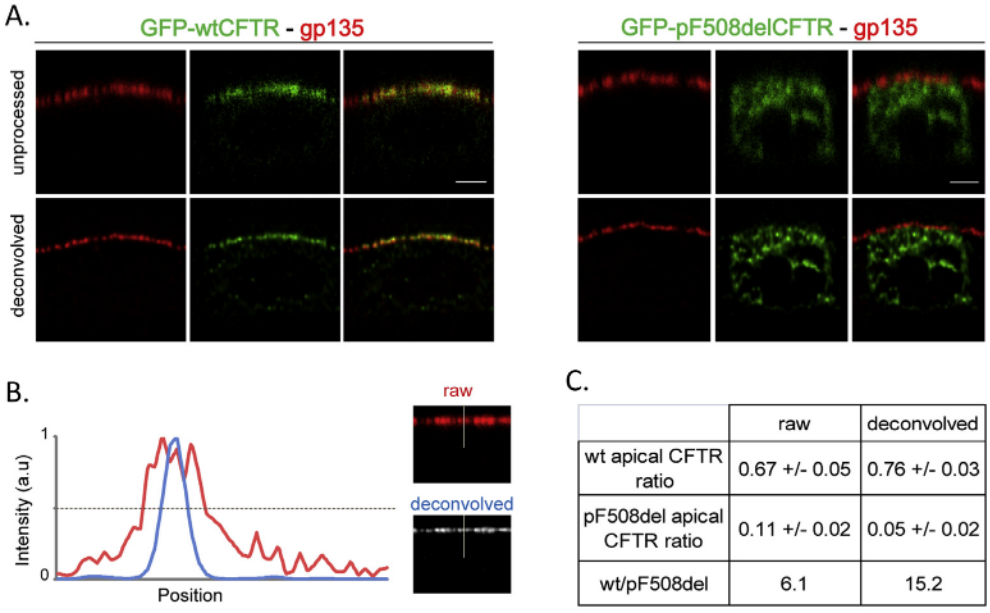

	raw	deconvolved
wt apical CFTR ratio	0.67 +/- 0.05	0.76 +/- 0.03
pF508del apical CFTR ratio	0.11 +/- 0.02	0.05 +/- 0.02
wt/pF508del	6.1	15.2

Fig. 3. Deconvolution of confocal images increases the dynamic range of the system. A. Distribution patterns of the apical marker gp135 and GFP-CFTR (both wt and pF508del) were already discernible in unprocessed images (upper panels) and improved by deconvolution (lower panels). Scale bars represent 3um. B. GFP-CFTR intensity patterns of a vector in xz confocal slice for unprocessed (red) or deconvolved (blue) images. The overlay demonstrates the similarity of the patterns. C. "Apical CFTR ratio" for wt and pF508del before and after deconvolution. Data represent mean ± standard deviation from at least three independent experiments. *$p < 0.0001$. Values of wt/pF508del ratio illustrate deconvolution increases by two and a half-fold the dynamic range of the system. (For interpretation of the references to color in this figure legend, the reader is referred to the web version of this article.)

aberration that increases with the observation depth [25]. We solved this difficulty by applying a theoretical psf, which can be adjusted to sample depth by deconvolution software calculation.

b) Signal to noise ratio (S/N): We first determined a range for this value (10 20) according to the quality of our images by visually estimating their granularity in comparison with confocal images of known S/N ratio. We then refined this value to 20, since after deconvolution, better axial resolution was obtained (Supplementary Fig. 1).

c) Number of maximum iterations and quality threshold criteria: The number of maximum iterations was kept high (500 iterations) making the quality threshold criteria the limiting factor for the iterative calculations. This latter value was set in 0.001, which additionally sharpened the intensity peak (Supplementary Fig. 1).

As shown in Fig. 3A, axial resolution, as indicated by the reduction in gp135 apical marker signal full width at half maximum (FWHM) value, increases almost by two-fold after deconvolution (note decrease in peak width, Fig. 3B). Noteworthy, intensity patterns of deconvolved images closely correspond to those obtained for unprocessed images. Hence deconvolution does not remove or create any artifactual features in the original images (Fig. 3B). After deconvolution, the apical CFTR ratios were 0.76 ± 0.03 for wild type and 0.05 ± 0.02 for pF508del, resembling the results previously reported (Fig. 3C) [23]. Thus, deconvolution expands the dynamic range of this measurement system (represented by wt/pF508del), offering a better resolution to discern populations with milder phenotypes.

3.5. Reported system accurately detects milder phenotypes

We further tested our system by measuring rescue of the pF508del phenotype by incubation at 27 °C. This condition has previously been reported to partially restore CFTR localization by overcoming protein folding-dependent ER retention and allowing the protein to proceed on its route to the plasma membrane [23].

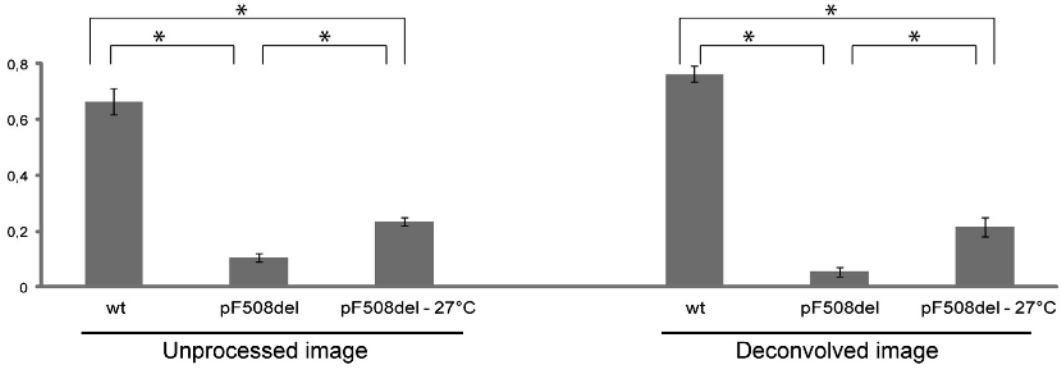

Fig. 4. Rescue of pF508del. To obtain pF508del-rescued phenotype, cells were incubated after transfection at 27 °C in a 5% CO_2 atmosphere for 24 h, and then used for the experiments. "Apical CFTR ratio" is represented for wt, pF508del and pF508del-27 °C for unprocessed and deconvolved images. Data represent mean ± standard deviation from at least three independent experiments. *$p < 0.0001$.

MDCK cells were transfected with EGFP-pF508del and incubated for 24 h at 27 °C (pF508del-27 °C). In accordance with previously reported data, our system detected a partial restoration of apical pF508del-27 °C, with an average ratio of 0.23 ± 0.01 or 0.22 ± 0.03 after deconvolution (Fig. 4).

Apical targeting of pF508del at 27 °C exhibits ratio values close to both wt and pF508del values. The distribution of pF508del-27 °C values might be due to cell to cell variability in the levels of the different cellular components needed for protein folding, quality control and subsequent delivery to the apical membrane [26]. We observed that whereas the average ratio of pF508del-27 °C before and after deconvolution is almost unchanged, there is a slight increase in its SD after deconvolution (see Supplementary Fig. 2). Restoring spatial information of the imaged objects increases imaging resolution and therefore it expands the distribution of data points due to cell to cell variation rendering a higher SD.

We conclude that this image analysis method is able to discriminate intermediate phenotypes, and therefore it is suitable for detecting mutations that mildly affect CFTR apical membrane targeting.

In comparison with other available methods for CFTR targeting estimation, ours is fast and straightforward without compromising sensitivity. In addition, our method can be extended to proteins that cannot be modified at extracellular domains and also to proteins that are internally associated to the cell membrane.

4. Conclusion

In this work we developed and validated an image analysis method to quantitatively examine CFTR at the apical membrane. This method reproduces previously reported results of CFTR localization and quantitatively detects partial protein localization restoration at the apical membrane. This method has good sensitivity, which can be further increased by deconvolution calculations. Therefore, it is suitable to identify mutations that either completely or mildly affect protein apical delivery. In contrast to whole population-based methods to quantify CFTR subcellular localization, this quantitative image analysis method retrieves single cell data, evidencing population heterogeneity that is otherwise hidden in a population average. Moreover, the analysis of approximately twenty cells per condition and experiment is sufficient to retrieve conclusive data. This method could be a valuable tool in the understanding of the effect of unknown mutations in CFTR. Additionally, it can be extended to other studies centered in the biology underlying protein compartmentalization in health and disease.

Acknowledgments

We thank Cecilia Larocca for critical reading of the manuscript and Magali San Cristobal for help with statistical analysis. This work was funded by Fondo María Viñas FMV_2009_1_2668 from Agencia Nacional de Investigación e Innovación (L.P.), Sistema Nacional de Becas (L.P, P.L.) and Sistema Nacional de Investigadores (A.K.).

Appendix A. Supplementary data

Supplementary data related to this article can be found at http://dx.doi.org/10.1016/j.mcp.2014.02.004

References

[1] Hung MC, Link W. Protein localization in disease and therapy. J Cell Sci 2011;124(Pt 20):3381–92.
[2] Riordan JR, Rommens JM, Kerem B, Alon N, Rozmahel R, Grzelczak Z, et al. Identification of the cystic fibrosis gene: cloning and characterization of complementary DNA. Science 1989;245(4922):1066–73.
[3] Rommens JM, Iannuzzi MC, Kerem B, Drumm ML, Melmer G, Dean M, et al. Identification of the cystic fibrosis gene: chromosome walking and jumping. Science 1989;245(4922):1059–65.
[4] Bobadilla JL, Macek Jr M, Fine JP, Farrell PM. Cystic fibrosis: a worldwide analysis of CFTR mutations–correlation with incidence data and application to screening. Hum Mutat 2002;19(6):575–606.
[5] Cheng SH, Gregory RJ, Marshall J, Paul S, Souza DW, White GA, et al. Defective intracellular transport and processing of CFTR is the molecular basis of most cystic fibrosis. Cell 1990;63(4):827–34.
[6] Krasnov KV, Tzetis M, Cheng J, Guggino WB, Cutting GR. Localization studies of rare missense mutations in cystic fibrosis transmembrane conductance regulator (CFTR) facilitate interpretation of genotype-phenotype relationships. Hum Mutat 2008;29(11):1364–72.
[7] Sheppard DN, Travis SM, Ishihara H, Welsh MJ. Contribution of proline residues in the membrane-spanning domains of cystic fibrosis transmembrane conductance regulator to chloride channel function. J Biol Chem 1996;271(25):14995–5001.
[8] Vankeerberghen A, Wei L, Jaspers M, Cassiman JJ, Nilius B, Cuppens H. Characterization of 19 disease-associated missense mutations in the regulatory domain of the cystic fibrosis transmembrane conductance regulator. Hum Mol Genet 1998;7(11):1761–9.
[9] Xiong X, Bragin A, Widdicombe JH, Cohn J, Skach WR. Structural cues involved in endoplasmic reticulum degradation of G85E and G91R mutant cystic fibrosis transmembrane conductance regulator. J Clin Invest 1997;100(5):1079–88.
[10] Tsui LC. Cystic fibrosis mutation database; 2007.
[11] Sosnay PR, Siklosi KR, Van Goor F, Kaniecki K, Yu H, Sharma N, et al. Defining the disease liability of variants in the cystic fibrosis transmembrane conductance regulator gene. Nat Genet, 45(10):1160–67.
[12] Pinton P, Tsuboi T, Ainscow EK, Pozzan T, Rizzuto R, Rutter GA. Dynamics of glucose-induced membrane recruitment of protein kinase C beta II in living pancreatic islet beta-cells. J Biol Chem 2002;277(40):37702–10.
[13] Stauffer TP, Ahn S, Meyer T. Receptor-induced transient reduction in plasma membrane PtdIns(4,5)P2 concentration monitored in living cells. Curr Biol 1998;8(6):343–6.
[14] Bush A, Colman-Lerner A. Quantitative measurement of protein relocalization in live cells. Biophys J, 104(3):727–36.
[15] Kasson PM, Huppa JB, Krogsgaard M, Davis MM, Brunger AT. Quantitative imaging of lymphocyte membrane protein reorganization and signaling. Biophys J 2005;88(1):579–89.
[16] Moyer BD, Denton J, Karlson KH, Reynolds D, Wang S, Mickle JE, et al. A PDZ-interacting domain in CFTR is an apical membrane polarization signal. J Clin Invest 1999;104(10):1353–61.
[17] Gentzsch M, Chang XB, Cui L, Wu Y, Ozols VV, Choudhury A, et al. Endocytic trafficking routes of wild type and DeltaF508 cystic fibrosis transmembrane conductance regulator. Mol Biol Cell 2004;15(6):2684–96.
[18] Sharma M, Pampinella F, Nemes C, Benharouga M, So J, Du K, et al. Misfolding diverts CFTR from recycling to degradation: quality control at early endosomes. J Cell Biol 2004;164(6):923–33.
[19] Almaca J, Dahimene S, Appel N, Conrad C, Kunzelmann K, Pepperkok R, et al. Functional genomics assays to study CFTR traffic and ENaC function. Methods Mol Biol 2011;742:249–64.
[20] Granio O, Norez C, Ashbourne Excoffon KJ, Karp PH, Lusky M, Becq F, et al. Cellular localization and activity of Ad-delivered GFP-CFTR in airway epithelial and tracheal cells. Am J Respir Cell Mol Biol 2007;37(6):631–9.
[21] Team RC. R: a language and environment for statistical computing. Vienna, Austria; 2012.
[22] Otsu N. A threshold selection method from gray-level histograms. IEEE Trans Syst Man Cybern 1979;1(9):5.
[23] Denning GM, Anderson MP, Amara JF, Marshall J, Smith AE, Welsh MJ. Processing of mutant cystic fibrosis transmembrane conductance regulator is temperature-sensitive. Nature 1992;358(6389):761–4.
[24] Sedarat F, Lin E, Moore ED, Tibbits GF. Deconvolution of confocal images of dihydropyridine and ryanodine receptors in developing cardiomyocytes. J Appl Phys 2004;97(3):1098–103.
[25] Biggs DS. 3D deconvolution microscopy. Curr Protoc Cytom 2010;19:11–20. Chapter 12:Unit 12.
[26] Loewer A, Lahav G. We are all individuals: causes and consequences of non-genetic heterogeneity in mammalian cells. Curr Opin Genet Dev, 21(6):753–758.